Monolayer graphene photonic metastructures: Giant Faraday rotation and nearly perfect transmission

Haixia Da,[1] Qiaoliang Bao,[2,3] Roozbeh Sanaei,[1] Jinghua Teng,[4] Kian Ping Loh,[5,6]
Francisco J. Garcia-Vidal,[7] and Cheng-Wei Qiu[1,*]

[1]*Electrical and Computer Engineering Department, National University of Singapore, 4 Engineering Drive 3, Singapore 117576, Singapore*
[2]*Institute of Functional Nano and Soft Materials (FUNSOM), Soochow University, Suzhou 215123, P. R. China*
[3]*Department of Materials Engineering, Monash University, Clayton Campus, Clayton, Victoria 3800, Australia*
[4]*Institute of Materials Research and Engineering, Agency for Science, Technology, and Research (A*STAR), 3 Research Link, Singapore 117602, Singapore*
[5]*Graphene Research Centre, National University of Singapore, 2 Science Drive 3, Singapore 117542, Singapore*
[6]*Department of Chemistry, National University of Singapore, 3 Science Drive 3, Singapore 117543, Singapore*
[7]*Departamento de Fisica Teorica de la Materia Condensada and Condensed Matter Physics Center (IFIMAC), Universidad Autonoma de Madrid, 28049 Madrid, Spain*

(Received 17 March 2013; revised manuscript received 15 October 2013; published 6 November 2013; corrected 25 August 2014)

We demonstrate a heterogeneous photonic metastructure involving monolayer graphene achieving a substantial Faraday rotation angle and nearly perfect transmittance simultaneously. This breaks the longstanding tradeoff between the Faraday rotation angle and the transmission coefficient in conventional magneto-optical devices. Faraday rotation is enhanced across the interface between two photonic crystals due to the presence of an interface mode, i.e. optical Tamm state, which presents a strong electromagnetic field confinement at the location of the graphene sheet. This interface mode also helps to maintain a nearly perfect optical transmission through the structure thanks to a resonant tunneling mechanism. This exciting result was achieved particularly in the quantum regime with low Fermi level.

DOI: 10.1103/PhysRevB.88.205405 PACS number(s): 81.05.ue, 78.20.Ls, 42.70.Qs

I. INTRODUCTION

Graphene has attracted considerable interest due to its unique optical properties, such as, transformation optics and plasmonics.[1–17] Another promising application of graphene is in magneto-optics. The opportunity of creating a giant Faraday rotation (FR) angle has been identified experimentally in both single-layer and multilayered graphene structures, which provides completely new candidates for producing magneto-optical (MO) effects.[18–23] The FR angle of graphene is a fascinating physical phenomenon that distinguishes from that observed in conventional bulky magnetic materials, in which the FR angle is proportional to the distance light travels. The reported experimental FR angle for a pristine or patterned graphene layer itself does not exceed 0.15 rad, which does not satisfy the demand of MO devices. On the other hand, graphene embedded in cavities has been found to be effective in achieving a larger FR angle.[19,20] However, due to the tradeoff between the FR angle and transmission, transmission rates of those reported graphene devices are usually low, which restricts their practical applications. It is then vital to find new routes to break the typical tradeoff in graphene-based devices.

Tamm states refer to interface electron states occurring within an energy band gap and are spatially located at a crystal surface.[24] Since the original concept proposed by Tamm *et al.*, there have been extensive studies on these modes in conventional semiconductors or metals.[25–27] In analogy with the electronic case, optical Tamm states (OTMs) have been explored in dielectric photonic crystals (PCs) and metamaterials.[28–31] Optical Tamm states have also greatly contributed to the development of the field of magneto-optics, as analyzed in Ref. 32. It is shown that the improved MO performance is due to the existence of OTMs located at the interface between the two subsystems. In contrast, such an effect is absent in simple periodic magneto-PCs due to the above-mentioned intrinsic tradeoff between the transmission and FR effect.[33,34] In this paper, multilayer bulky magnetic materials are used to tune the phase, and thus an accumulated FR angle is achieved. However, single-layer graphene almost has no ability of tune the phase due to its atomic thickness. To explore the effective configuration with only single-layer graphene enabling good MO performance is significant for the application of graphene in MO devices.

In this paper, we theoretically report a simultaneously improved FR angle and high optical transmission in a graphene-based heterogeneous PC (G-HPC). By appropriately manipulating the parameters of the two types of PCs, the amplitude of the FR angle (transmission) can be made as large as -10.9° (0.85) at chosen operating frequency. The physical mechanism behind the good MO performance is revealed by the combination of an effective refraction model and the analysis of the electromagnetic field distributions. Additionally, the spectral position of the large FR angle in graphene, which is intrinsically sensitive to the external magnetic field via a square-root dependence, is suppressed in G-HPCs due to the resonant character of the OTMs involved.

II. METHODOLOGY

A schematic picture of the proposed structure (G-HPC) is shown in Fig. 1. The single-layer graphene lies in the x-y plane, which is sandwiched between the two PCs. Labels A, B, C and D represent four isotropic dielectric materials and m and n are the repetition numbers of the A/B and C/D subsystems, respectively. An external magnetic field (B) is applied along the z direction. For proof-of-principle purposes,

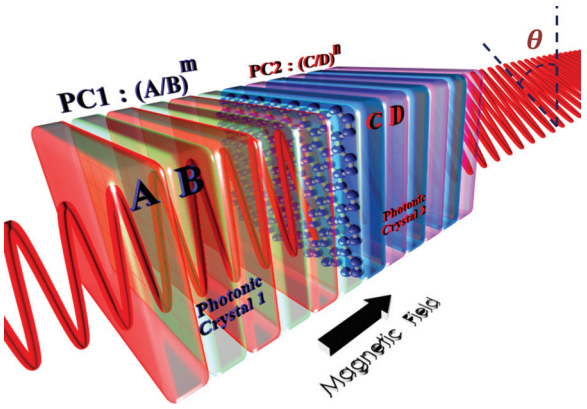

FIG. 1. (Color online) Schematic diagram of the proposed structure, where graphene is sandwiched by PC1 and PC2. An external magnetic field is perpendicular to the graphene sheet.

we consider silicon as the dielectric material for both A and C components, whereas SiC is the one used for both B and D. The refractive indexes of SiO_2 and SiC for the range of frequencies analyzed are 1.5 and 2.55, respectively.[35] The thicknesses of the four PC components are taken as $d_A = 4.99\ \mu$m, $d_B = 1.39\ \mu$m; $d_C = 0.95\ \mu$m and $d_D = 3.77\ \mu$m to operate at the specific working frequency of 25 THz. The chosen thicknesses of the components are related to the existence of an OTM acquired by the phase matching condition $r_L r_R = 1$,[36] where r_L and r_R are reflection coefficients of the left and right periodic structures with wave impinging from vacuum, respectively (see Appendix A for details). Regarding the optical properties of graphene, it is worth mentioning that, as a difference with some previous experimental works on Faraday rotation in graphene-based structures,[18,21] here, we operate in the so-called quantum regime by taking a very low Fermi energy $\mu = 4$ meV. Here, ac conductivity of graphene is introduced via Kubo formula[37] (see Appendix B for details).

III. RESULTS AND DISCUSSIONS

Numerical calculations of both the FR angle and optical transmission were performed by employing the transfer matrix method.[38] Figures 2(a) and 2(b) show the FR angle θ_p and transmission at B = 1 T in a G-HPC structure under normal incidence. The results of the G/SiC structure (graphene on top of a SiC substrate with thickness of 1.39 μm), PC1, and PC2 are also shown for comparison. Here, θ_p is zero for both PC1 and PC2 due to the components' reciprocity, while there is a pronounced enhancement in θ_p at the specific frequency of 25 THz in the G-HPC structure. Its spectral location falls within the frequency band-gap region of two PCs. The peak value of θ_p is -0.27° and the corresponding transmission is very high, 0.98. The FR angle shown here is about 8 times larger than that of G/SiC structure, and it also yields a greatly increased transmission, going from 0.48 to 0.98. Thus, the important feature here is that enhanced θ_p and high transmission are achieved simultaneously, indicating the traditional tradeoff is lifted.

It is insightful to reveal the physical mechanism that dominates good performance in the G-HPC structure. This can be understood in terms of the effective circular birefringence of the hybrid structure. To this end, we thus calculate the right circularly polarized (RCP) light and left circularly polarized (LCP) light transmission coefficients t_{++} and t_{--}. Transmission spectra for both RCP ($T_{++} = |t_{++}|^2$) and LCP ($T_{--} = |t_{--}|^2$) lights are shown in Fig. 2(c). The result of the G/SiC structure is also shown. It has no prominent features, while there are three resonances in the G-HPC transmission spectra for both RCP and LCP lights. At the three resonances, the peak of RCP transmission amplitude approaches almost 1 and is larger than that of LCP light. Moreover, the RCP and LCP peaks acquire the maximum values at slightly different frequencies, indicating a different phase modulation of the G-HPC structure for the two different polarizations. We can correlate these resonant features in the transmission spectrum with the density of optical modes (DOM) in the

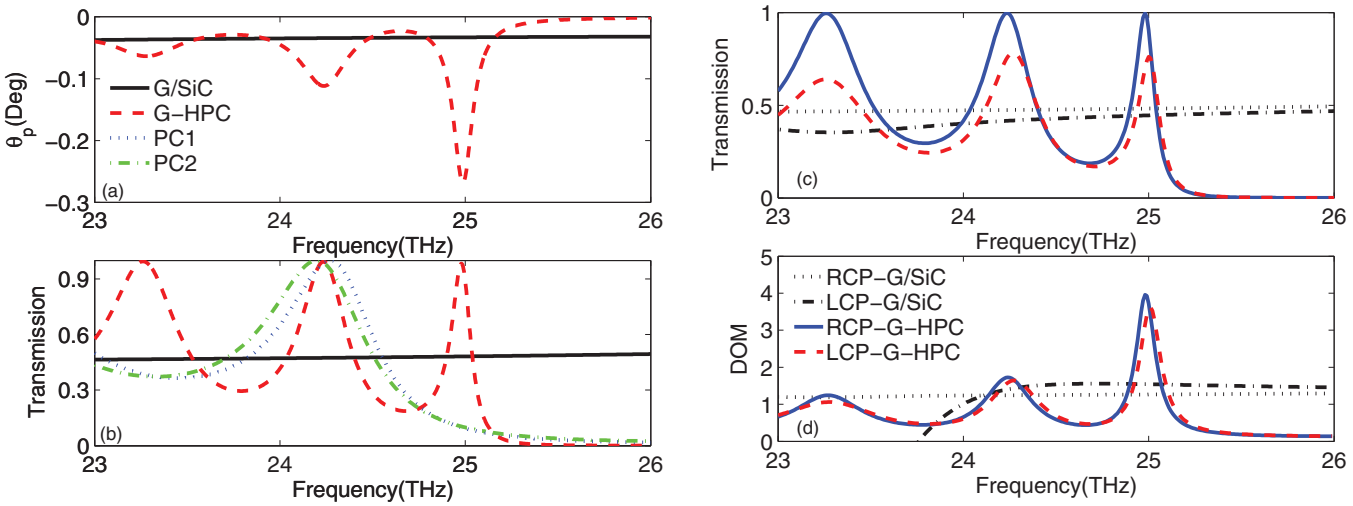

FIG. 2. (Color online) (a) The FR angle. (b) Transmission versus frequency in the G/SiC and G-HPC structures and two bare PCs, where $m = n = 6$. (c) The transmission and (d) the corresponding DOM in arbitrary units for RCP and LCP lights in the G/SiC and G-HPC structures, respectively.

structure. This physical parameter carries information of the availability of allowed photonic states within a certain frequency range, entering into the electromagnetic dynamics via the derivative of photonic dispersion relationship.[39] In our finite system, DOM is determined by the derivative of the effective wave vector parallel to the propagating direction.[40] Figure 2(d) shows the DOM versus frequency for RCP and LCP components. The DOM value of the G/SiC structure is enlarged by 100 times for visualization at the same scale. As expected, the G/SiC structure does not exhibit any resonant effect, thus leading to a broadband small FR angle. In G-HPC structure, the DOM of RCP and LCP lights oscillate over the 23–26 THz frequency range. Two small DOM peaks appear at frequencies corresponding to a Fabry-Perot resonance (23.3 THz) and band-edge transmission resonance (24.3 THz). The DOM achieves the maximum value at 25 THz, which is related to the significant decrease of the group velocities and thus the strongly spatial localization of light at the interface between the two PCs. Besides, slightly different localization conditions emerge around the specified working frequency for effectively RCP and LCP lights due to their different propagation velocities. Consequently, the designed G-HPC structure has an intrinsic contribution to modulate the effective RCP and LCP lights, thus generating a large FR angle.

A. Field distribution

It is meaningful to visualize the role of the HPC structure in improving graphene's MO performance. In Fig. 3, we plot the spatial profiles of the electric field in HPC and G-HPC structures at the excitation frequency of 25 THz, respectively. Panels (a) and (b) present the electric field distributions of $|E_x|$ and $|E_y|$ for the HPC configuration without graphene in between. The most important feature is that there is no E_y component in the absence of graphene, indicating that no propagating wave gets rotated in the polarization plane of the incident wave. Furthermore, the electric (and magnetic as well, not shown) fields reach local maxima at the center of each A/B component within PC1 rather than at the interfaces of the A-B bilayers. There are two local maxima also within each component of the PC2, and the E_x component of the field intensity of the wave in PC2 is overall smaller than that in PC1. Close to the interface between PC1 and PC2, the electric field reaches the global maximum value. Both the electric and magnetic fields are exponentially decaying within the two PCs away from the interface, which indicates that a standing wave emerges allowing the resonant tunneling of light through the whole structure.

In contrast to the HPC structure without graphene, Figs. 3(c) and 3(d) show that the propagating wave through the G-HPC structure has not only an E_x component but also an E_y component, despite the fact that the incident wave had only an E_x component. The electric field enhancement in E_x and E_y components appear in an alternating pattern within the two PCs. It reveals that the polarization plane of the transmitted wave gets rotated due to the gyrotropy effect of graphene. Besides, the electric field amplitude reaches its maximum near to the interface between the two PCs and the decaying wave penetrates into several layers into the two PCs. The field intensity is localized, to a large extent, at the center of the whole

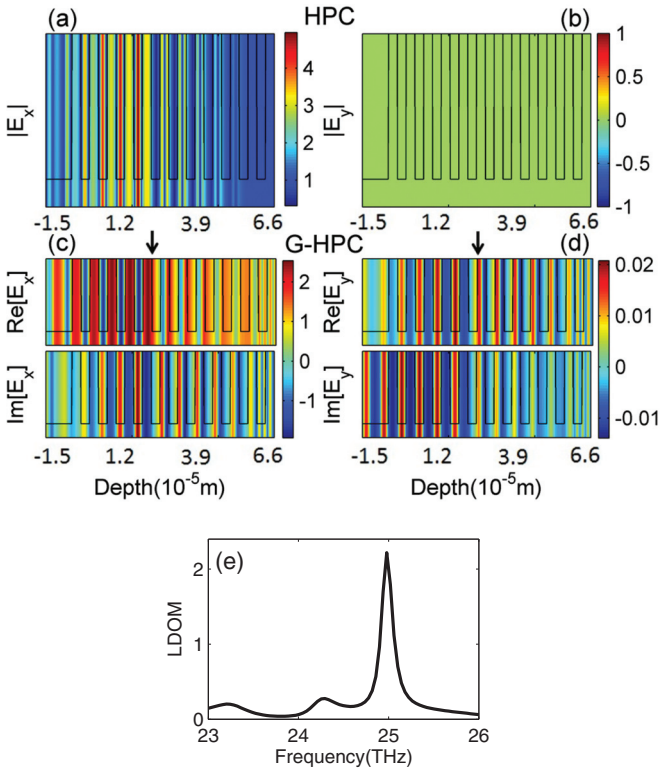

FIG. 3. (Color online) Electric field intensity distribution (a) $|E_x|$ and (b) $|E_y|$ across the HPC structure without graphene; The real and imaginary parts of electric intensity distribution (c) E_x and (d) E_y across the G-HPC structure. The arrows show the location of graphene, and the solid line represents the refractive index profile. (e) LDOM in arbitrary units versus frequency at the specific location where the graphene sheet stays.

structure where the single atomic layer graphene is located, suggesting that the enhanced MO effects originate from the electromagnetic field localization. The strong interference between forward and backward propagating waves leads again to a standing wave and thus a robust localized interface mode, the OTM, which increases the coupling between the incident wave and graphene. Therefore, the FR angle per unit of wave propagation length along G-HPC structure is obviously large even for a monolayer graphene due to the confinement of resonant states. This resonant tunneling of an electromagnetic wave is empowered by OTMs that determines the enhanced FR angle and its associated high transmission. The key role played by the OTM is illustrated in Fig. 3(e), which shows the local density of modes (LDOM) versus frequency evaluated at the location of the graphene sheet.[41] A close correspondence between the spectral locations in which FR is enhanced and the resonant peaks in the LDOM is observed.

B. Magnetic field dependence of the FR in the quantum regime

In the quantum regime, the Dirac character of carriers in graphene leads to a cyclotron resonance that increases with the B field following a square-root dependence.[6] It enables another degree of freedom to optimize MO performance.

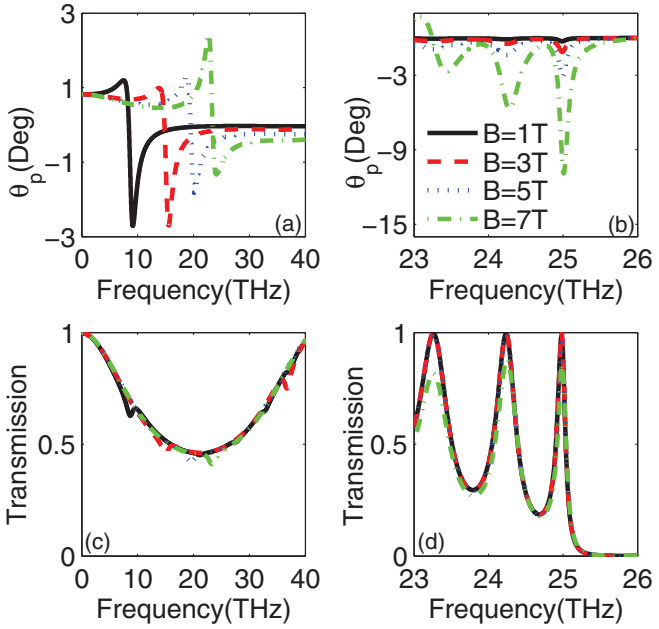

FIG. 4. (Color online) (a) The FR angle and (c) transmission versus frequency in the G/SiC structure; (c) the FR angle and (d) transmission versus frequency in the G-HPC structure.

Figures 4(a) and 4(c) represent θ_p and transmission in the G/SiC structure when the B field varies from 1 to 7 T. Clearly, there is a dip in the FR angle for each individual B field, and the dip's position shifts toward higher frequencies following the square-root dependence of the B field. The corresponding transmission spectra are not sensitive to the B field, and transmission is always less than 0.65 for the maximum FR angle. Figures. 4(b) and 4(d) show θ_p and transmission of the proposed G-HPC structure, respectively. Our results imply that increased B field further enhances θ_p (-10.9° at B = 7 T) but does not degrade the transmission too much, i.e. it decreases from 0.98 to 0.85 when the B field increases from 1 to 7 T.

As explained above, the confined character of the interface OTM results in a large θ_p in contrast to that in the G/SiC structure. The enhancement of θ_p with the B field can be traced back to the relativistic Landau levels quantization of graphene.[1] The value of θ_p is closely related to the real part of σ_{xy}, Re[σ_{xy}]. The value of Re[σ_{xy}] gets larger with the magnitude of the B field at the specific 25 THz. For example, the magnitude of Re[σ_{xy}] at B = 7 T is almost 40 times larger than that at B = 1 T. The combination of the strong field confinement along with localized mode and increased Re[σ_{xy}] of graphene results in a further enhancement in θ_p at high B field. Regarding the transmission spectrum, its magnitude is mainly dictated by the designed PC structure and, therefore, much less sensitive to the B field. This behavior is very much different from the case of the two-layer structure, in which the position of the FR dip varies with the B field.[18,21] This distinction may be understood because the enhanced FR angle in the G-HPC structure is mainly determined by spectral location of the OTM that has a structural/dielectric origin and not by the cyclotron resonance.

C. Extension to other frequency

Thus, the G-HPC structure can enhance the MO performance of graphene at a desirable working frequency given appropriate geometric arrangement of the two PCs. The mechanism is applied to other frequencies by simply modifying the structural parameters. For example, the improved MO effect can be achieved using the same Si and SiC as in previous calculations but changing the structural parameters to $d_A = 4.20\ \mu$m, $d_B = 2.61\ \mu$m; $d_C = 3.62\ \mu$m, and $d_D = 2.95\ \mu$m to operate at lower frequency 9.5 THz. The FR angle increases from 0.28° further to 5.58°, and transmission increases from 0.48 to 0.98 at B = 1 T when going from the G/SiC to the G-HPC structure. Finally, the MO performance here survives at oblique incidence but slightly degrades compared with the case of normal incidence. We emphasize that the designed structure governs the nature of the desirable MO effect. The high transmission can be guaranteed by the applied phase match condition. One direct proof is the field distribution, where strong field is observed to localize at the interface along with the existence of the interface mode. The nonreciprocity of graphene in the presence of a magnetic field breaks the degeneracy of RCP and LCP waves, whose phase difference can be strongly enlarged at the designed structure and thus offers the condition of achieving a large FR angle extrinsically.

D. Effects of stacking sequence on FR and the transmission

It has been reported that the sequence of components is vital to determine the appearance of OTMs.[36] Figures 5(a) and 5(b) demonstrate the FR angle and transmission spectrum for HPC structure with different arrangement sequence of components. As expected, resonant tunneling disappears when we only swap the sequence of layers within each PC due to the broken phase matching condition. However, as shown in Fig. 5, there is a dip in the θ_p spectrum, and a corresponding transmission peak appears in the (B/A)graphene(D/C) structure, signifying

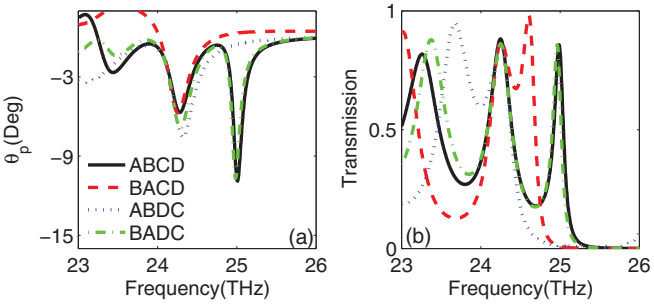

FIG. 5. (Color online) The effect of sequence in PCs on the appearance of resonant tunneling is considered for different combined sequences of components. (a) The FR angle and (b) transmission are plotted as a function of frequency in the G-HPC structure. Solid, dash, dotted, and dash-dotted lines illustrate the FR angle and transmission of $(A/B)^m$/graphene/$(C/D)^n$, $(B/A)_m$/graphene/$(C/D)_n$, $(A/B)_m$/graphene/$(D/C)_n$, and $(B/A)_m$/graphene/$(D/C)_n$, respectively. There is no resonant tunneling in $(B/A)_m$/graphene/$(C/D)_n$ and $(A/B)_m$/graphene/$(D/C)_n$ due to the broken phase matching condition. Resonant tunneling survives when the sequence of components in both PCs is changed, indicating that the existence of the localized mode is not sequence independent.

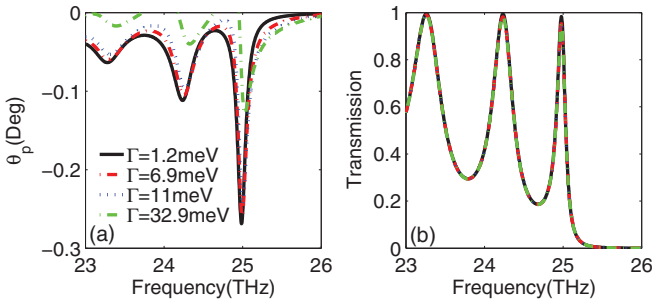

FIG. 6. (Color online) (a) The FR angle and (b) transmission as a function of frequency in the G-HPC structure at different broadening parameters, where the magnetic field is set to be 1 T.

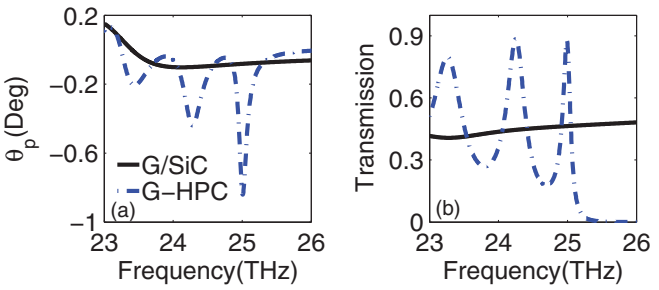

FIG. 7. (Color online) Room temperature MO performance of the systems. (a) The FR angle and (b) transmission as a function of frequency in the G/SiC and G-HPC structures at room temperature, where the magnetic field is set to be 7 T. Solid and dash lines illustrate the FR angle and transmission for the G/SiC and G-HPC structures, respectively.

that the resonant tunneling survives when swapping the layer sequence in both PCs. Therefore, if the sequences of both PC components vary, the spatial distribution of electric and magnetic intensity is expected to vary, but the localized interface mode remains the same and thus a relatively large FR angle and transmission survive in the modified structure.

E. Effect of the broadening parameter on MO performance

Considering the available experimental technique on obtaining graphene, such as the chemical vapor deposition (CVD) based method, we investigate the effect of the broadening parameter on MO performance, as shown in Figs. 6(a) and 6(b). The broadening parameter Γ is chosen to be 6.6 (100), 11.0 (60), and 32.9 (20) meV(fs), corresponding to cases of different quality CVD grown graphene.[42,43] The other parameters are chosen to be the same as Fig. 2(a) in the text. The result of the original broadening parameter 1.2 (550) meV(fs) is also shown for comparison. We can see that the peak of the FR angle (-0.27°) stays almost the same when Γ increases from 1.2 to 11.0 meV, and it then decreases to -0.12° for normal quality CVD grown graphene at the working frequency 25 THz. However, there is no obvious change in the transmission spectrum with an increased broadening parameter. It can be ascribed to the fact that the transmission in our configuration is determined by the resonant tunneling, and it is not very sensitive to graphene's parameter due to its atomic thickness. Our results imply that the quality of graphene grown by CVD method affects the FR angle slightly, but transmission stays almost the same. Therefore, high transmission along with a large FR angle survives with an increased broadening parameter.

F. Room temperature MO performance

Temperature is an issue which affects the device performance. A higher FR angle is expected at a lower temperature; thus, it is instructive to explore the MO performance at room temperature for real applications in MO devices. Using the theoretical method listed above, we calculated the FR angle and transmission as a function of frequency at room temperature 300 K, where the B field is fixed to be 7 T, and the other parameters are kept the same as Fig. 2(a) in the text. The room temperature MO response is shown in Fig. 7, and the results of the G/SiC configuration are also shown for comparison. It can be observed that the overall transmission of the G-HPC structure is not sensitive to temperature, but the FR angle can be engineered by the temperature. As expected, the FR angle gets smaller as the temperature increases from 10 to 300 K. Despite this fact, we found that the FR angle of the G-HPC structure can reach -0.8°, which is ten times larger than that of the G/SiC case and comparable to the value in conventional bulk magnetic materials.[32] These results can be understood as follows. The transmission is mainly determined by the designed PC structure and thus has a small dependence on the parameters of graphene. This temperature modulation effect on the FR angle is a direct consequence of the variations of ac conductivity in graphene due to thermal broadening effect. The real part of the off-diagonal ac term $\mathrm{Re}[\sigma_{xy}]$ at room temperature is only one-twelfth of the value at $T = 10$ K. In contrast to the low-temperature case, the high temperature tends to smear the original sharp peak out and thus leads to the degradation of the FR angle, whereas the transmission is insensitive to it. The sign of the FR angle is closely related to $\mathrm{Re}[\sigma_{xy}]$ and can be reversed upon the reversal of the magnetic field direction, which has been demonstrated in experiments.[44] Such a feature is still valid in our designed structure, which is not unusual and can be observed in conventional magnetic materials. Our results here indicate that the designed structure provides the opportunity to obtain the coexistence of a good FR angle and high transmission together, even at room temperature and avoids patterning graphene.[45,46]

IV. CONCLUSION

In summary, we have theoretically demonstrated giant MO effect in a metastructure with a graphene monolayer, in which a giant FR angle and high transmission are achieved simultaneously. Their coexistence is markedly distinguished from the currently existing graphene devices in which the tradeoff between those two physical magnitudes plays a key role in their performance. Such counterintuitive improvement in our structure is due to the existence of optical Tamm states occurring at the interface between the two PCs. It is well known that most of the MO materials lack tunability due to their invariable properties, which imposes serious restrictions to the applications in tunable optoelectronics, such as optical switches and displays. In contrast to conventional MO devices, the FR angle introduced by graphene can be controlled by external means, such as chemical potential and/or magnetic

fields.[47–52] Importantly, the magnitude of the FR peak increases with the magnetic field, but its spectral location is determined by the interface mode and is then insensitive to the magnetic field. Our proposed scheme opens a promising avenue to realize high-performance graphene MO devices that can be extended to other two-dimensional structures, such as silicene and transition metal dichalcogenides.

ACKNOWLEDGMENTS

This work was supported by the TDSI/11-004/1A and IMRE/12-1P0903. We thank Dr. Ding Weiqiang for useful discussions. F.J.G.-V acknowledges financial support from the European Research Council (ERC-2011-AdG Proposal No. 290981) and the Spanish MINECO under contract MAT2011-28581-C02-01. Q.B. acknowledges the support from the 863 Program (2013AA031903), NSFC (51222208, 51290273), ARC DECRA and MCN Technology Fellowship/ANFF-Victoria.

APPENDIX A: THE CONDITION OF THE EXISTENCE OF OTMS IN HETEROGENEOUS PC

The case of a homogeneous layer introduced by two virtual interfaces is employed to derive the condition of the existence of OTMs.[36] The relation between a left propagating wave at the left interface and a right propagating wave at the right interface can be connected by the propagating matrix. Its diagonal term is the phase factor $\exp(\pm i\omega/c\Delta x)$, where positive/negative sign represents the right/left propagating wave. Here, ω is the angular frequency of the incident wave, and c is the velocity of light in the vacuum. Also, Δx is the distance between two virtual layers. The combination of the continuity of the tangential component of electric field and $\Delta x = 0$ determines the condition of the existence of OTMs, i.e. $r_L r_R = 1$. Here, r_L and r_R are reflection coefficients of the left and right periodic structures with wave impinging from a vacuum, respectively. When there are two stacked PCs, the following equation should be satisfied to realize the OTMs:[53]

$$\xi_A \frac{[\xi_B \cos(k_{zA}d_A) + i\xi_A \sin(k_{zA}d_A)]\exp(ik_{zB}d_B) - \xi_B \exp[ik_{b1}(d_A + d_B)]}{[\xi_A \cos(k_{zA}d_A) + i\xi_B \sin(k_{zA}d_A)]\exp(ik_{zB}d_B) - \xi_A \exp[ik_{b1}(d_A + d_B)]} = \xi_C \frac{[\xi_D \cos(k_{zC}d_C) + i\xi_C \sin(k_{zC}d_C)]\exp(ik_{zD}d_D) - \xi_D \exp[ik_{b2}(d_C + d_D)]}{[\xi_C \cos(k_{zC}d_C) + i\xi_D \sin(k_{zC}d_C)]\exp(ik_{zD}d_D) - \xi_C \exp[ik_{b2}(d_C + d_D)]}, \tag{A1}$$

where d_i (i = A,B,C,D) is the thickness of each component in PCs, k_{zi} (i = A,B,C,D) is the wave vector along the z direction, i is an imaginary unit, and k_{bi} (i = 1,2) is the Bloch wave vector in PC.

APPENDIX B: DERIVATIONS OF FR AND THE TRANSMISSION IN MULTILAYERED STRUCTURE

Upon the application of the B field, graphene has the asymmetrical ac conductivity which can be obtained according to the Kubo formalism:[37]

$$\sigma_{\alpha\beta}(\Omega) = \frac{e^2}{2\omega}\int_{-\infty}^{+\infty}\frac{d\omega}{2\pi}[f(\omega-\mu) - f(\omega+\Omega-\mu)] \times \int\frac{dk^2}{(2\pi)^2} Tr[v_\alpha A(\omega+\Omega,\vec{k}) v_\beta A(\omega,\vec{k})],$$

($\alpha,\beta = x,y$), where $f(x) = \frac{1}{\exp[x/T]+1}$ is the Fermi-Dirac function and T/μ is the temperature/chemical potential. Here, Tr is the trace, and $A(\omega)$ is the spectral function, connected to the electronic Green's function $G_{ij}(z)$ by $G_{ij}(z) = \int_{-\infty}^{+\infty}\frac{d\omega}{2\pi}\frac{A_{ij}(\omega')}{z-\omega'}$. Also, $v_{\alpha,\beta}$ is the velocity matrix obtained by the derivatives of the Hamiltonian via Peierls substitution. The broadening parameter is assumed to be 1.2 meV, and the temperature is 10 K.[3] We assume that graphene is grown on Si-terminated surface of SiC and thus consider the MO effects in quantum regime. To this end, we use the following method to connect the relation between the incoming and outgoing wave functions and compare the present results with those in conventional MPC systems with bulky magnetic materials.

In the presence of ac conductivity ($\vec{\vec{\sigma}}$), the fundamental Maxwell's equation is presented by:

$$\nabla(\nabla\cdot\vec{E}) - \nabla^2\vec{E} = \frac{\omega^2}{c^2}\varepsilon_0\vec{E} + \frac{4\pi i\omega}{c^2}\vec{j}, \tag{B1}$$

where ε_0 stands for the contribution from ion to dielectric constant, and $\vec{j} = \vec{\vec{\sigma}}\cdot\vec{E}$ is the current induced by ac conductivity. Unlike conventional isotropic materials, it generally has four waves in a typical biaxial media, two of which are forward left- and right-handed circularly polarized propagating waves and another two are the corresponding backward propagating waves.

The incident wave vector can be expressed as $k_i = k_0(v_x, v_y, v_z)$, where $k_0 = \omega/c$. Here, c is the velocity of light in the vacuum. An electromagnetic wave impinges on the proposed structure with an angle θ_i confined in the x-z plane. It indicates $k_y = 0$, $v_x = n_i\sin(\theta_i)$, and $v_z = n_i\cos(\theta_i)$. The amplitude of electric field inside the biaxial media can be written as

$$E = E^p\hat{n}_p + E^s\hat{n}_s, \tag{B2}$$

where $\hat{n}_p$ and $\hat{n}_s$ are the unit vectors of linear polarizations. Here, $E^{p(s)}$ stands for the corresponding electric field component of $p(s)$ linear polarization.

The right- and left-going waves can be related by

$$\begin{pmatrix} E_t^p \\ E_t^s \end{pmatrix} = \begin{pmatrix} t_{pp} & t_{ps} \\ t_{sp} & t_{ss} \end{pmatrix}\begin{pmatrix} E_i^p \\ E_i^s \end{pmatrix}, \tag{B3}$$

where t_{ij} is the ratio of the incident j-polarized electric field and the transmitted i-polarized electric field. Here,

$E_i{}^{p(s)}$ and $E_t{}^{p(s)}$ are the electric field components of the incident and transmitted waves, respectively. The Ambartsumian's method is employed to obtain the reflection and transmission:[40]

$$R_j = r_j + \tilde{t}_j R_{j-1}(I - \tilde{r}_j R_{j-1})^{-1} t_j, \tag{B4}$$

$$T_j = T_{j-1}(I - \tilde{r}_j R_{j-1})^{-1} t_j, \tag{B5}$$

where $R_j(R_{j-1})$ and T_j (T_{j-1}) are the reflectance and transmittance matrices in the j $(j-1)$ biaxial layer, respectively. Here, r_j and t_j are the analogical matrices for the jth anisotropic layer, and the matrices with tildes are corresponding matrices for the reversed light propagation. The equations of $R_0 = 0$ and $T_0 = 1$ are satisfied.

Combining the ac conductivity of graphene and standard electrodynamics, one can obtain the FR angle by

$$\Theta_p = \theta_p + i\eta_p = \frac{t_{ps}}{t_{pp}}, \tag{B6}$$

where θ_p and η_p are the FR angle and the ellipticity for the p-polarized wave, respectively.

*chengwei.qiu@nus.edu.sg

[1] N. Stander, B. Huard, and D. Goldhaber-Gordon, Phys. Rev. Lett. **102**, 026807 (2009).

[2] J. Chen, M. Badioli, P. Alonso-González, S. Thongrattanasiri, F. Huth, J. Osmond, M. Spasenović, A. Centeno, A. Pesquera, P. Godignon, A. Z. Elorza, N. Camara, F. Javier García de Abajo, R. Hillenbrand, and F. H. L. Koppens, Nature **487**, 77 (2012).

[3] M. C. Lemme, T. J. Echtermeyer, M. Baus, and H. Kurz, IEEE Electron Device Lett. **28**, 282 (2007).

[4] S. Thibault and Y. Bin, Appl. Phys. Lett. **98**, 213104 (2011).

[5] F. Bonaccorso, Z. Sun, T. Hasan, and A. C. Ferrari, Nature Photonics **4**, 611 (2010).

[6] Y. Zhang, Y.-W. Tan, H. L. Stormer, and P. Kim, Nature **438**, 201, (2005).

[7] Q. Bao, H. Zhang, B. Wang, Z. Ni, C. H. Y. Xuan Lim, Y. Wang, D. Y. Tang, and K. P. Loh, Nature Photonics **5**, 411 (2011).

[8] A. Vakil and N. Engheta, Science **332**, 1291 (2011).

[9] M. Liu, X. Yin, E. Ulin-Avila, B. Geng, T. Zentgraf, L. Ju, F. Wang, and X. Zhang, Nature **474**, 64 (2011).

[10] V. V. Cheianov, V. Falko, and B. L. Altshuler, Science **315**, 1252 (2007).

[11] F. H. L. Koppens, D. E. Chang, and F. Javier García de Abajo, Nano Lett. **11**, 3370 (2011).

[12] A. Yu. Nikitin, F. Guinea, F. J. Garcia-Vidal, and L. Martin-Moreno, Phys. Rev. B **84**, 161407 (2011).

[13] Z. Y. Fang, S. Thongrattanasiri, A. Schlather, Z. Liu, L. L. Ma, Y. M. Wang, P. Ajayan, P. Nordlander, and J. H. Naomi, ACS Nano **7**, 2388 (2013).

[14] P.-Y. Chen and A. Alu, ACS Nano **5**, 5855 (2011).

[15] Q. Bao and K. P. Loh, ACS Nano **6**, 3677 (2012).

[16] Z. Y. Fang, Y. M. Wang, Z. Liu, A. Schlather, P. M. Ajayan, F. H. L. Koppens, P. Nordlander, and J. H. Naomi, ACS Nano **6**, 10222 (2012).

[17] Z. Y. Fang, Z. Liu, Y. M. Wang, P. M. Ajayan, P. Nordlander, and J. H. Naomi, Nano Lett. **12**, 3808 (2012).

[18] I. Crassee, J. Levallois, A. L. Walter, M. Ostler, A. Bostwick, E. Rotenberg, T. Seyller, D. van der Marel, and A. B. Kuzmenko, Nature Physics **7**, 48 (2011).

[19] Aires Ferreira, J. Viana-Gomes, Yu. V. Bludov, V. Pereira, N. M. R. Peres, and A. H. Castro Neto, Phys. Rev. B **84**, 235410 (2011).

[20] H. Da and G. Liang, Appl. Phys. Lett. **98**, 261915 (2011).

[21] I. Crassee, M. Orlita, M. Potemski, A. L. Walter, M. Ostler, Th. Seyller, I. Gaponenko, J. Chen, and A. B. Kuzmenko, Nano Lett. **12**, 2470 (2012).

[22] H. G. Yan, Z. Q. Li, X. S. Li, W. J. Zhu, P. Avouris, and F. N. Xia, Nano Lett. **12**, 3766 (2012).

[23] D. L. Sounasa and C. Calozb, Appl. Phys. Lett. **98**, 021911 (2011).

[24] I. E. Tamm, Physik Z. Sowjetunion **1**, 733 (1932).

[25] C. Grossmann, C. Coulson, G. Christmann, I. Farrer, H. E. Beere, D. A. Ritchie, and J. J. Baumberg, Appl. Phys. Lett. **98**, 231105 (2011).

[26] E. Homeyer, C. Symonds, A. Lemaitre, J.-C. Plenet, and J. Bellessa, Superlattice Microst **49**, 224 (2011).

[27] M. N. Read, Phys. Rev. B **75**, 193403 (2007).

[28] N. Malkova and C. Z. Ning, Phys. Rev. B **76**, 045305 (2007).

[29] R. Brückner, M. Sudzius, S. I. Hintschich, H. Fröb, V. G. Lyssenko, and K. Leo, Phys. Rev. B **83**, 033405 (2011).

[30] A. Namdar, I. V. Shadrivov, and Y. S. Kivshar, Appl. Phys. Lett. **89**, 114104 (2006).

[31] A. Namdar, S. R. Entezar, H. Tajalli, and Z. Eyni, Opt. Express **16**, 10543 (2008).

[32] T. Goto, A. V. Dorofeenko, A. M. Merzlikin, A. V. Baryshev, A. P. Vinogradov, M. Inoue, A. A. Lisyansky, and A. B. Granovsky, Phys. Rev. Lett. **101**, 113902 (2008).

[33] M. J. Steel, M. Levy, and R. M. Osgood, IEEE Photonics Technol. Lett. **12**, 1171 (2000).

[34] M. J. Steel, M. Levy, and R. M. Osgood, J. Lightwave Technol. **18**, 1289 (2000).

[35] A. R. Forouhi and I. Bloomer, Phys. Rev. B **38**, 1865 (1988).

[36] M. Kaliteevski, I. Iorsh, S. Brand, R. A. Abram, J. M. Chamberlain, A. V. Kavokin, and I. A. Shelykh, Phys. Rev. B **76**, 165415 (2007).

[37] V. P. Gusynin and S. G. Sharapov, Phys. Rev. B **73**, 245411 (2006).

[38] A. H. Gevorgyan, Phys. Rev. E **85**, 021704 (2012).

[39] I. Alvarado-Rodrıguez, P. Halevi, and J. J. Sanchez-Mondragon, Phys. Rev. E **59**, 3624 (1999).

[40] G. D'Aguanno, N. Mattiucci, M. Scalora, M. J. Bloemer, and A. M. Zheltikov, Phys. Rev. E **70**, 016612 (2004).

[41] G. Boedecker and C. Henkel, Opt. Express **11**, 1590 (2003).

[42] J. Horng, C.-F. Chen, B. Geng, C. Girit, Y. Zhang, Z. Hao, H. A. Bechtel, M. Martin, A. Zettl, M. F. Crommie, Y. R. Shen, and F. Wang, Phys. Rev. B **83**, 165113 (2011).

[43] J. H. Strait, H. Wang, S. Shivaraman, V. Shields, M. Spencer, and Farhan Rana, Nano Lett. **11**, 4902 (2011).

[44] P. Neugebauer, M. Orlita, C. Faugeras, A. L. Barra, and M. Potemski, Phys. Rev. Lett. **103**, 136403 (2009).

[45] M. Tymchenko, A. Yu. Nikitin, and L. Martin-Moreno, ACS Nano. (2013), doi: 10.1021/nn403282x.

[46] A. Fallahi and J. Perruisseau-Carrier, Appl. Phys. Lett. **101**, 231605 (2012)
[47] J. C. Martinez and M. B. A. Jalil, Europhys. Lett. **96**, 27008 (2011).
[48] N. Ubrig, I. Crassee, J. Levallois, I. O. Nedoliuk, F. Fromm, M. Kaiser, T. Seyller, and A. B. Kuzmenko, Opt. Express **21**, 24736 (2013).
[49] D. L. Sounas, H. S. Skulason, H. V. Nguyen, A. Guermoune, M. Siaj, T. Szkopek, and C. Caloz, Appl. Phys. Lett. **102**, 191901 (2013).
[50] H. Da and C. W. Qiu, Appl. Phys. Lett. **100**, 241106 (2012).
[51] R. Shimano, G. Yumoto, J. Y. Yoo, R. Matsunaga, S. Tanabe, H. Hibino, T. Morimoto, and H. Aoki Nat. Commun. **4**, 1841 (2013).
[52] I. Fialkovsky and D. V. Vassilevich, Eur. Phys. J. B **85**, 384 (2012).
[53] A. P. Vinogradov, A. V. Dorofeenko, S. G. Erokhin, M. Inoue, A. A. Lisyansky, A. M. Merzlikin, and A. B. Granovsky, Phys. Rev. B **74**, 045128 (2006).